AMERICAN SOCIETY FOR MICROBIOLOGY | Journal of Virology®

Deletion of the Vaccinia Virus I2 Protein Interrupts Virion Morphogenesis, Leading to Retention of the Scaffold Protein and Mislocalization of Membrane-Associated Entry Proteins

Seong-In Hyun,[a,b] Andrea Weisberg,[a] Bernard Moss[a]

Laboratory of Viral Diseases, National Institute of Allergy and Infectious Diseases, National Institutes of Health, Bethesda, Maryland, USA[a]; Department of Cell Biology and Molecular Genetics, University of Maryland, College Park, Maryland, USA[b]

ABSTRACT The I2L open reading frame of vaccinia virus (VACV) encodes a conserved 72-amino-acid protein with a putative C-terminal transmembrane domain. Previous studies with a tetracycline-inducible mutant demonstrated that I2-deficient virions are defective in cell entry. The purpose of the present study was to determine the step of replication or entry that is affected by loss of the I2 protein. Fluorescence microscopy experiments showed that I2 colocalized with a major membrane protein of immature and mature virions. We generated a cell line that constitutively expressed I2 and allowed construction of the VACV I2L deletion mutant vΔI2. As anticipated, vΔI2 was unable to replicate in cells that did not express I2. Unexpectedly, morphogenesis was interrupted at a stage after immature virion formation, resulting in the accumulation of dense spherical particles instead of brick-shaped mature virions with well-defined core structures. The abnormal particles retained the D13 scaffold protein of immature virions, were severely deficient in the transmembrane proteins that comprise the entry fusion complex (EFC), and had increased amounts of unprocessed membrane and core proteins. Total lysates of cells infected with vΔI2 also had diminished EFC proteins due to instability attributed to their hydrophobicity and failure to be inserted into viral membranes. A similar instability of EFC proteins had previously been found with unrelated mutants blocked earlier in morphogenesis that also accumulated viral membranes retaining the D13 scaffold. We concluded that I2 is required for virion morphogenesis, release of the D13 scaffold, and the association of EFC proteins with viral membranes.

IMPORTANCE Poxviruses comprise a large family that infect vertebrates and invertebrates, cause disease in both in humans and in wild and domesticated animals, and are being engineered as vectors for vaccines and cancer therapy. In addition, investigations of poxviruses have provided insights into many aspects of cell biology. The I2 protein is conserved in all poxviruses that infect vertebrates, suggesting an important role. The present study revealed that this protein is essential for vaccinia virus morphogenesis and that its absence results in an accumulation of deformed virus particles retaining the scaffold protein and deficient in surface proteins needed for cell entry.

KEYWORDS complementing cell, deletion mutant, electron microscopy, mutant virus, poxviruses, virus assembly

Received 2 April 2017 **Accepted** 5 May 2017

Accepted manuscript posted online 10 May 2017

Citation Hyun S-I, Weisberg A, Moss B. 2017. Deletion of the vaccinia virus I2 protein interrupts virion morphogenesis, leading to retention of the scaffold protein and mislocalization of membrane-associated entry proteins. J Virol 91:e00558-17. https://doi.org/10.1128/JVI.00558-17.

Editor Grant McFadden, The Biodesign Institute, Arizona State University

Address correspondence to Bernard Moss, bmoss@nih.gov.

Poxviruses are large, double-stranded DNA viruses that replicate entirely in the cytoplasm of infected cells (1). Morphogenesis begins with the formation of crescent membranes that enlarge to form spherical immature virus particles (IVs), which

are then transformed into brick-shaped mature virions (MVs) (2). Studies with vaccinia virus (VACV), the prototype of the poxvirus family, indicate that 60 to 80 viral proteins are associated with the core and membrane fractions of MVs (3–6). These proteins enable virus attachment to the cell, fusion of viral and cellular membranes, and early gene expression. A complex of 11 small transmembrane (TM) proteins of the MV is required for the membrane fusion step of virus entry and is therefore known as the entry-fusion complex or EFC (7, 8). Recently, an additional protein encoded by the I2L open reading frame (ORF) of VACV, with homologs in all chordopoxviruses, was reported to be essential for virus entry, although a physical association with the EFC was apparently not investigated (9). The I2 protein is predicted to have 72 amino acids with a calculated mass of 8.4 kDa and a C-terminal TM domain. The protein is synthesized following viral DNA replication and is associated with purified MVs (6, 9). Using a recombinant VACV with a tetracycline-inducible I2L ORF, Nichols et al. (9) showed that repression of I2L results in a profound reduction in virion infectivity due to the inability of the virions to enter cells. These researchers noted a reduction in several EFC components in the viral membrane but considered this unlikely to account for the large decrease in the specific infectivity of I2-deficient virions, although this possibility was not entirely discounted.

The purpose of the present study was to further analyze the role of the I2 protein in VACV replication. Our starting point was the production of a cell line that expresses the I2 protein and allowed the construction of an I2L deletion mutant by homologous recombination. We found that this null mutant had a primary block in virion assembly, which prevented the release of the D13 scaffold and the association of the EFC proteins with viral membranes, leading to their instability.

(The research conducted by S.-I.H. was in partial fulfillment of the Ph.D. requirements of the Biological Sciences Graduate Program at the University of Maryland, College Park, MD.)

RESULTS

Intracellular localization of I2. The association of I2 with purified virus particles was previously shown by Western blotting using an epitope tag antibody (9) and by mass spectroscopy (4, 6). We were interested in determining its intracellular localization since this might help to further investigate its role. Because a useful antibody to I2 was not available, the recombinant virus vGFP-I2 was made by replacing the I2L ORF of the VACV Western Reserve strain (vWR) with DNA encoding green fluorescent protein (GFP) fused to the N terminus of I2, while retaining the natural I2 promoter. Since I2 is an essential protein, the ability of vGFP-I2 to replicate well in RK-13 cells provided evidence that the fusion protein retained function. At 8 h after the infection of RK-13 cells, GFP fluorescence was detected by confocal microscopy in DAPI (4′,6′-diamidino-2-phenylindole)-stained viral factories adjacent to nuclei and outside the large factories as small dots probably representing individual virus particles or small clusters of them (Fig. 1A). GFP-I2 colocalized in factories and in individual dots with A14, a major membrane component of IVs and MVs (Fig. 1A). GFP-I2 also localized with the I7 proteinase, which is responsible for cleaving the A17 membrane protein, as well as core proteins, in the factories, but little I7 was detected in the dots (Fig. 1B), perhaps because of small amounts or poor access of the antibody within MVs. There was only partial colocalization of I2 and A11 (Fig. 1C), a protein that associates with the growing edge of IVs and is not found in appreciable amounts in MVs (10, 11). Some overlap of GFP-I2 fluorescence with the endoplasmic reticulum markers calnexin and protein disulfide isomerase (PDI) was detected but only within the factory area (not shown). Attempts to localize GFP-I2 by transmission electron microscopy of immunostained cryosections were unsuccessful probably because of its relatively low abundance (data not shown). Based on the confocal microscopy, we concluded that I2 is primarily associated with IVs and MVs.

Construction of an I2L deletion mutant. Because repression of gene expression by inducible mutants is not always stringent, we decided to construct an I2L deletion

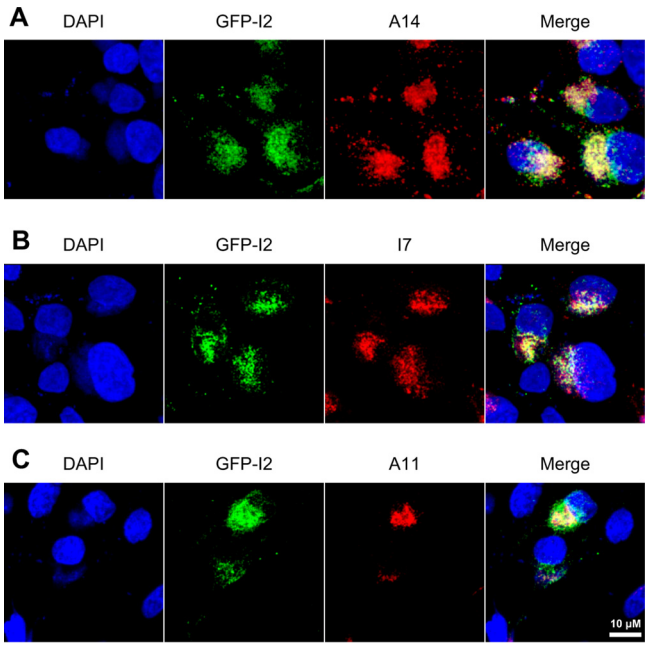

FIG 1 Intracellular localization of the I2 protein. RK-13 cells were infected with 3 PFU/cell of vGFP-I2 for 8 h and then fixed and stained with mouse MAb to A14 (A) or with rabbit PAbs to I7 (B) or A11 (C), followed by secondary staining with donkey anti-mouse or goat anti-rabbit antibody conjugated to Alexa Fluor 568 or 647 and with DAPI. Because of the relatively low multiplicity of infection, some cells remained uninfected. The 10-μm scale bar shown in the bottom right applies to all panels.

mutant. However, since the I2 protein is essential for replication, it was first necessary to make a cell line that expresses I2 and can complement a virus-null mutant. We chose rabbit kidney RK-13 cells because they are permissive for VACV and have previously been used to make complementing cell lines that express other VACV proteins (12, 13). A eukaryotic codon-optimized version of the I2L ORF with a N-terminal hemagglutinin (HA) tag was incorporated into a lentiviral vector, which was then used for gene delivery to RK-13 cells (Fig. 2A). Transduced cells were isolated by antibiotic selection and clonally purified. Western blotting (Fig. 2B) and fluorescence microscopy (Fig. 2C) demonstrated expression of HA-I2 in the cytoplasm of the RK-HA-I2 cells.

To delete the I2L ORF of VACV, DNA encoding GFP regulated by the VACV late P11 promoter was flanked by sequences upstream and downstream of I2L (Fig. 3A) and transfected into RK-HA-I2 cells that were infected by VACV to allow homologous recombination. The mutant viruses formed green fluorescent plaques on RK-HA-I2 cells and were clonally purified by repeated plaque picking. Loss of the I2L ORF was confirmed by sequencing. As expected, vΔI2 was unable to form plaques in the parental RK-13 cells or in BS-C-1 cells (Fig. 3B). At high magnification, single RK-13 cells infected with vΔI2 could be detected by their fluorescence, but spread to neighboring cells did not occur (Fig. 3C). Furthermore, vΔI2 replicated in RK-HA-I2 cells but not in RK-13 cells (Fig. 3D), although the virus titers in the former were generally less than that of vWR (data not shown).

Replication of vΔI2 was blocked during morphogenesis. RK-13 and RK-HA-I2 cells were infected with vΔI2 and examined by transmission electron microcopy to determine whether there was visible evidence of alterations in the growth cycle. Unexpectedly, we discovered that morphogenesis was altered in noncomplementing RK-13 cells. The cytoplasm contained large factory areas, within which were normal-looking IVs but an absence of brick-shaped MVs (Fig. 4A and B). Instead of MVs, there were numerous dense spherical viral particles (DVs), which were like IVs in size and shape. At higher magnifications, some of the DVs had rudimentary core structures (shown below). In contrast, IVs and MVs with well-defined cores formed in RK-HA-I2

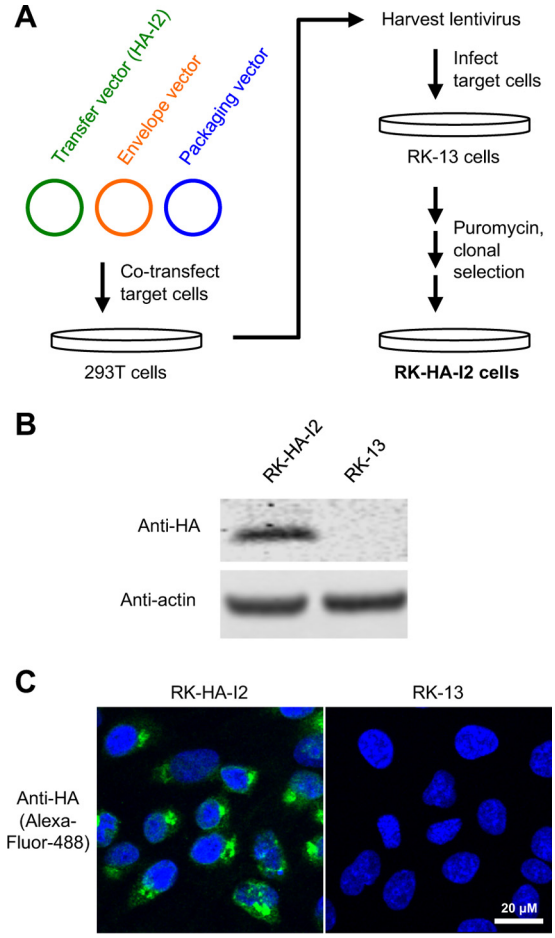

FIG 2 Construction and selection of a RK-HA-I2 cell line. (A) Diagram of lentiviral transduction method used for making the RK-HA-I2 cell line. Western blot analysis (B) and immunofluorescence labeling (C) were used to confirm the expression of HA-I2 in the selected RK-HA-I2 cell line alongside its parent RK-13 cell line as control. Scale bar, 20 μm.

cells infected with vΔI2 (Fig. 4C and D), demonstrating that the effect on morphogenesis could be overcome solely by the expression of I2. By manually counting particles in thin sections of 100 RK-13 cells at 18 h after infection, we found a higher ratio of IVs to DVs (1,096/797) for vΔI2 than IVs to MVs (659/2,397) for vWR. A similar block in morphogenesis occurred in BS-C-1 cells infected with vΔI2 (not shown). The particles purified by sedimentation through a sucrose cushion and banding on a CsCl gradient from RK-13 cells infected with vΔI2 retained their spherical shape (Fig. 4F), which was distinct from the brick shape of MV particles purified from cells infected with vWR (Fig. 4E). The negative staining procedure does not allow the distinction of IVs and DVs, which have the same size and shape. However, the appearance of the particles in the preparation of MVs suggests that IVs were not recovered by this purification procedure.

During a normal infection, the transformation of spherical IVs to brick-shaped MVs is accompanied by disassembly of the external scaffold formed by trimers of the D13 protein (14, 15). The latter step is associated with the processing of the A17 membrane protein that interacts with the D13 trimers (16, 17). Antibody to the D13 protein, followed by protein A conjugated to gold spheres, was used to localize the scaffold protein in RK-13 and RK-HA-I2 cells infected with vΔI2. D13 was associated with the IVs and the DVs in RK-13 cells (Fig. 5A and B). The rudimentary core structures of two DVs in Fig. 5B were well visualized by the cryosectioning electron microscopic technique. In RK-HA-I2 cells, D13 was also associated with IVs but not MVs (Fig. 5C and D), which have lost D13 during the transition from a spherical to a brick shape. Thus, I2 deficiency

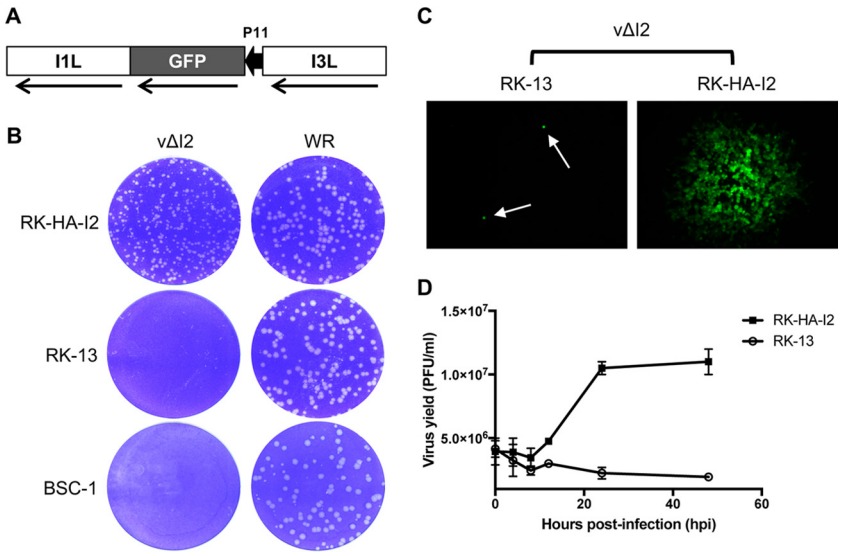

FIG 3 I2 is essential for virus spread. (A) Diagram of vΔI2 genome showing the replacement of the I2L ORF by P11 promoter-regulated GFP and the flanking I3L and I1L ORFs. (B) Plaque formation by vΔI2 and vWR. RK-HA-I2, RK-13, and BS-C-1 cells were infected with vΔI2 or vWR. At 48 hpi, the infected cells were washed and stained with crystal violet. (C) Enlarged fluorescent plaque images. RK-13 and RK-HA-I2 cells were infected with vΔI2 as in panel B. At 48 hpi, the cells were imaged with a fluorescence microscope. White arrows indicate cells infected with vΔI2, which failed to spread to neighboring cells. (D) One-step growth curves of vΔI2. RK-HA-I2 and RK-13 cells were infected with 3 PFU/cell of vΔI2. The infected cells were collected at 0, 4, 8, 12, 24, and 48 hpi. The virus titers for each time point were determined by plaque assay using RK-HA-I2 cells. The individual values (bars) and the means for two independent experiments are shown.

prevented the removal of the D13 scaffold and further steps of morphogenesis. The accumulation of DVs retaining D13 was previously noted when the synthesis of the I7 protease was repressed (16).

I2-deficient virus particles have small amounts of EFC proteins. Nichols et al. (9) previously analyzed the proteins associated with I2–deficient virus particles formed in the absence of the tetracycline inducer. By Western blotting, these researchers found normal amounts of most proteins but an ~5-fold decrease in A21, G3, and A28, which are each components of the EFC. We carried out a similar comparison of vΔI2 and wild-type (WT) virus particles assembled in RK-13 cells. Electron micrographs of the purified particles are shown in Fig. 4E and F. Specific antibodies were used to analyze 15 proteins, of which 7 were components of the EFC, 7 were other membrane and core proteins, and 1 was the D13 scaffold protein. There was, on average, a 10-fold reduction in the amount of each EFC protein in the I2-deficient virus particles compared to the amounts in WT virus particles (Fig. 6A). In contrast, there were similar amounts of the other proteins with one striking exception: a 30-fold increase in D13 in I2-deficient virus particles (Fig. 6B). This result was consistent with the immunogold D13 labeling of the DVs (Fig. 5A and B). Another notable difference was greater amounts of unprocessed A3 and A17 proteins seen as higher bands in the Western blots (Fig. 6B), a further sign of a perturbation in morphogenesis.

Decreased accumulation of EFC proteins in vΔI2-infected RK-13 cells. The decreased amounts of EFC proteins in the virus particles could be due to their diminished synthesis, instability, or failure to be transported to particles. To investigate these possibilities, lysates of RK-13 cells infected with WT VACV or vΔI2 and of RK-HA-I2 cells infected with vΔI2 were analyzed by SDS-PAGE and Western blotting. The pattern of abundant viral proteins appeared indistinguishable when the blot was probed with antiserum from rabbits that were infected with VACV (18), indicating the absence of a general effect on viral protein synthesis (Fig. 7A). However, there were smaller amounts of the EFC proteins in RK-13 cells infected with vΔI2 compared to vWR (Fig. 7B).

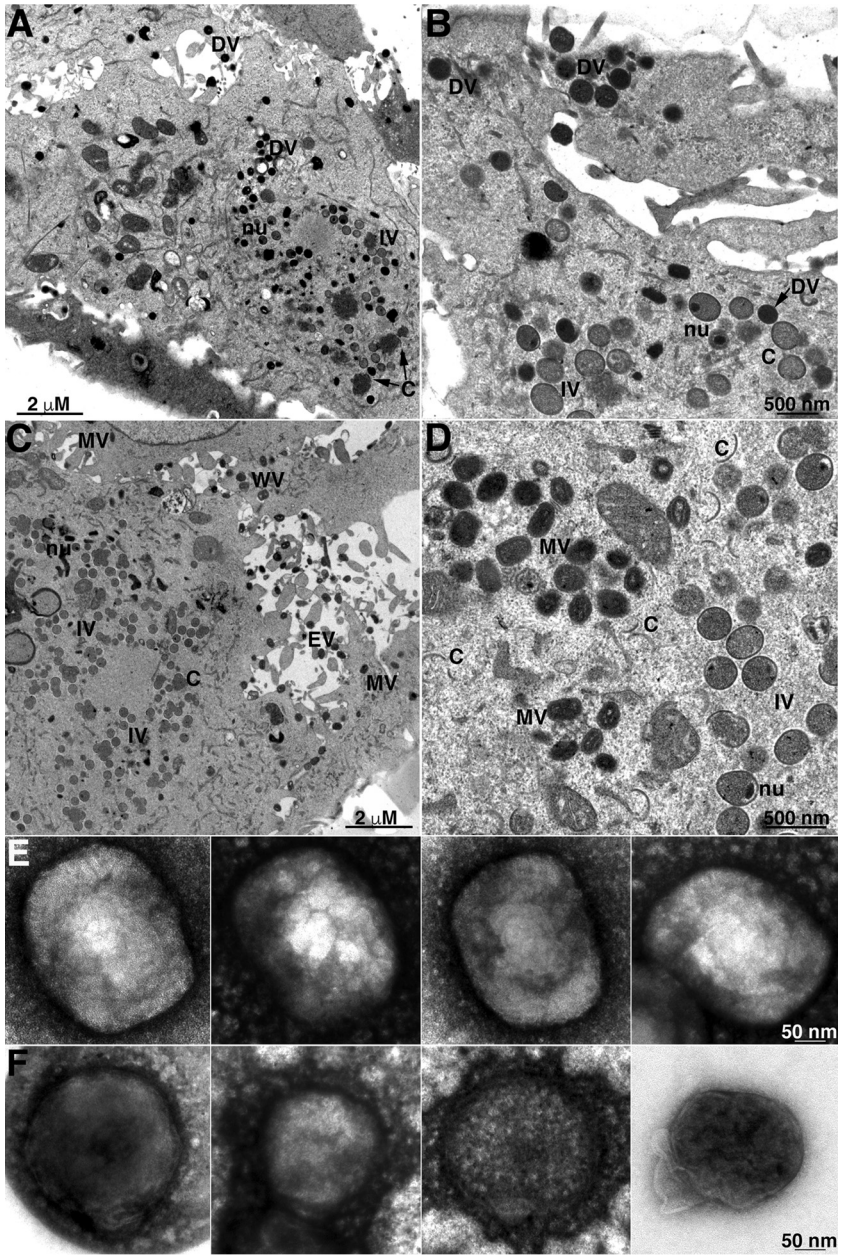

FIG 4 Transmission electron micrographs of cells infected with vΔI2 and purified virus particles. RK-13 cells (A and B) and RK-HA-I2 cells (C and D) were infected with 3 PFU/cell of vΔI2. At 18 hpi, the cells were harvested, fixed, and prepared for transmission electron microscopy. Virus particles from RK-13 cells infected for 18 h with WT vWR (E) or mutant vΔI2 (F) virus were purified by sedimentation through a sucrose cushion and banding in a CsCl gradient. Abbreviations: C, crescent; DV, dense spherical virion; IV, immature virion; nu, IV with nucleoid; MV, mature virion; WV, wrapped virion.

Although there was some variation, the difference was ~4-fold on average. This effect was partially overcome when RK-HA-I2 cells expressing I2 were infected with vΔI2 (Fig. 7B). In contrast, there were similar amounts of non-EFC proteins in the cells infected with vWR and vΔI2, although we noted greater amounts of unprocessed A3 and A17 in cells infected with vΔI2 (Fig. 7C). We also compared the levels of the scaffold protein D13 and I7, the proteinase responsible for cleavage of both A3 and A17 and needed for disassembly of D13, in RK-13 cells infected with vΔI2. Although D13 was present in similar amounts, I7 was reduced ~3-fold (Fig. 7D).

The small amounts of the EFC proteins could be due to diminished synthesis or protein instability. To distinguish between these possibilities, we carried out digital PCR

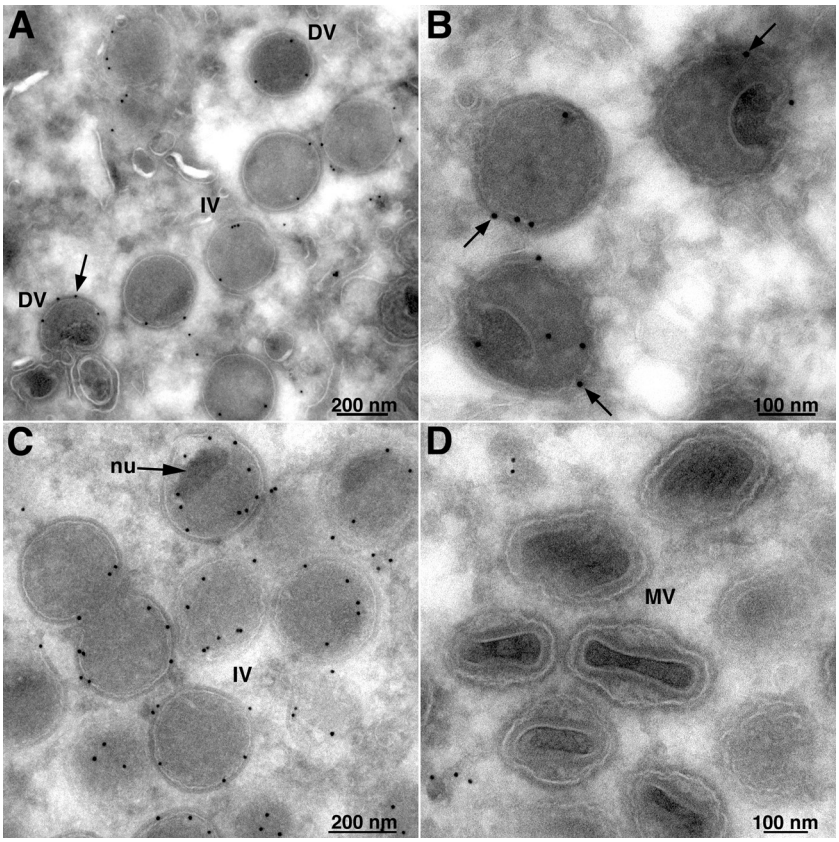

FIG 5 Immuno-electron microscopic images showing localization of D13 in IVs and DVs. RK-13 cells (A and B) and RK-HA-I2 cells (C and D) were infected with 3 PFU/cell of vΔI2. Cells were collected at 18 hpi for fixation and preparation for immune-electron microscopy using primary polyclonal antibody to D13, followed by protein A-gold. Arrows point to gold spheres. Abbreviation: nu, nucleoid within IV.

to determine mRNA levels and pulse-labeling with radioactive amino acids to determine protein synthesis and stability. There were only small differences in the amounts of viral mRNAs encoding EFC and non-EFC proteins in RK-13 cells infected with vWR or vΔI2, suggesting that the difference in protein levels did not have a transcriptional basis (Fig. 8A). We analyzed the synthesis and stability of L1 and F9 proteins because of the availability of suitable antibodies for immunoaffinity capture. After a 5-min labeling period, the intensity of the L1 and F9 bands from RK-13 cells infected with vWR and vΔI2 were similar. However, the proteins made in the cells infected with vΔI2 decreased more rapidly during a 2-h chase, indicating lower stability (Fig. 8B).

DISCUSSION

Nichols et al. (9) previously reported that the I2L gene encodes a membrane protein with an essential role in virion entry. We were interested in extending this study to determine the stage of entry that was affected and therefore constructed an I2L deletion mutant for high stringency rather than an inducible mutant. In several previous studies (12, 13, 19, 20), VACV mutants with deletions of essential genes were made and propagated in complementing cell lines that express the missing gene. We introduced an HA-tagged I2 gene regulated by a eukaryotic promoter into RK-13 cells using a lentivirus vector and screened antibiotic-resistant mutants for expression of the HA tag. Cell lines constitutively expressing HA-I2 in the cytoplasm were isolated, and one was used to construct a VACV mutant with a deletion of the I2L ORF by homologous recombination and to propagate the mutant virus. As anticipated, the virus was unable to replicate in cells not expressing I2, confirming the requirement for this protein. We were surprised, however, to discover a profound block in morphogenesis

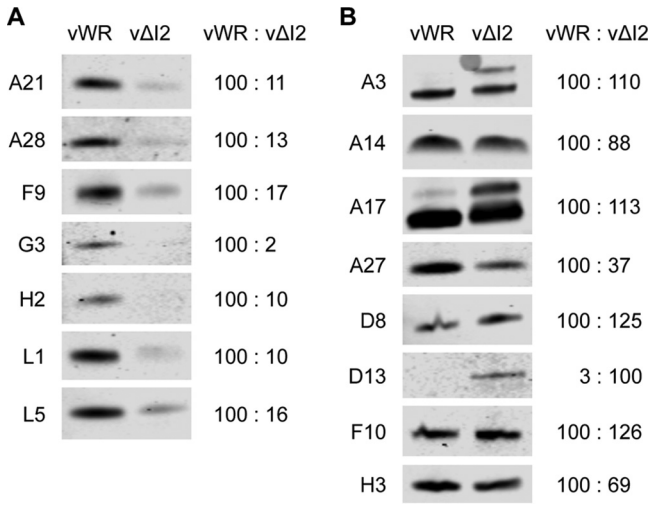

FIG 6 Proteins in purified virus particles. Lysates were prepared from RK-13 cells infected with vWR or vΔI2, and virus particles were purified by sedimentation through a sucrose cushion, followed by CsCl centrifugation. The purified virus particles were dissociated, and the proteins were resolved by SDS-PAGE and transferred to membranes. The blots were probed with antibodies to seven individual VACV EFC proteins (A) and to eight non-EFC membrane, core, and scaffold proteins (B). The VACV protein targets of the antibodies are indicated on the left, and the relative band intensities are indicated on the right. The band intensities were normalized to 100 for vWR except for the D13 protein, which was normalized to 100 for vΔI2.

that had not been noted in a previous study with an inducible I2 mutant in BSC-40 cells (9). In the present study, the IVs appeared normal, but spherical dense viral particles accumulated instead of brick-shaped MVs. Although these particles contained normal amounts of most core and membrane proteins, they were greatly deficient in EFC proteins, had an increased amount of the D13 scaffold protein, and had increased

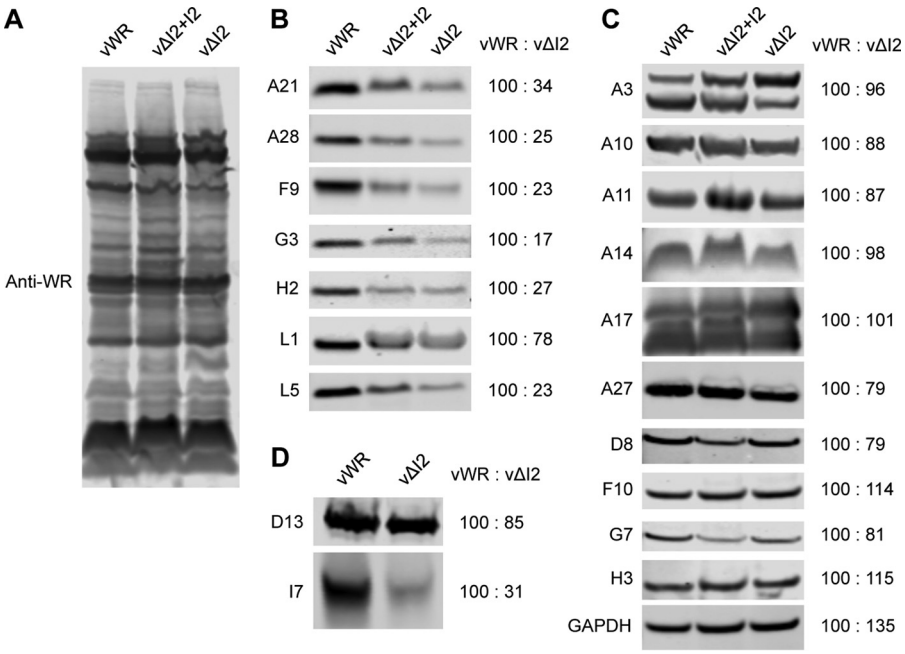

FIG 7 Viral proteins in total cell extracts. RK-13 cells were infected with 3 PFU/cell of vWR (left lane) or vΔI2 (right lane), and RK-HA-I2 cells were infected with 3 PFU/cell of vΔI2 (middle lane in panels A, B, and C). After 20 h, the proteins of total cell lysates were resolved by SDS-PAGE, transferred to membranes, and probed with antibodies to vWR (A), EFC proteins (B), other membrane and core proteins and a GAPDH loading control (C), and D13 and I7 (D).

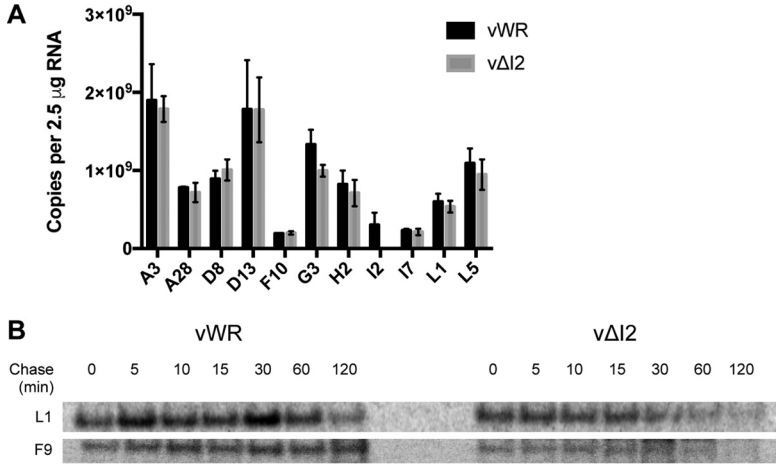

FIG 8 Expression of EFC mRNAs and proteins. (A) mRNA levels. RK-13 cells were infected at a multiplicity of 10 PFU/cell with vWR or vΔI2. At 10 hpi, RNA was extracted from infected cells and reverse transcribed to cDNA. Primers for indicated genes were used for digital PCR, and the number of copies of each mRNA in 2.5 μg of total RNA was determined. The individual values (bars) and the means for two independent experiments are shown. (B) Pulse-chase experiment. RK-13 cells were infected with 5 PFU/cell of vWR or vΔI2. At 6 hpi, the cells were pulse-labeled with 100 μCi of [^{35}S]methionine-cysteine for 5 min in methionine-cysteine-deficient medium and then chased in label-free normal medium. At the indicated time, lysates were prepared, and L1 and F9 proteins were immunopurified with specific antibodies and analyzed by SDS-PAGE and autoradiography.

amounts of unprocessed A3 and A17 proteins. Thus, failure to disassemble the scaffold appeared to be a major defect that was previously reported to occur when I7, the proteinase responsible for the cleavage of A17, as well as several core proteins, was repressed (16). Interestingly, there was a reduced amount of I7 in cytoplasmic extracts of RK-13 cells infected with vΔI2 further, suggesting some relationship between the two proteins.

The EFC proteins have either N- or C-terminal transmembrane domains but lack signal peptides, and their modes of insertion into the viral membrane are not yet understood. However, previous electron microscopic studies showed that in contrast to A17, which is detected in both IVs and MVs, L1 is only detected in MVs, suggesting that insertion of the EFC proteins may occur after removal of the D13 scaffold (21). In the present study, we found that the EFC proteins were also diminished when the total cell lysate was analyzed, although not as drastically as in purified virus particles. A specific diminution in EFC proteins was previously noted when the formation of IVs was impaired due to deletion or repression of individual viral membrane assembly proteins (VMAPs), notably A6, A11, A30.5, H7, and L2 (10, 11, 19, 20, 22–24). A common feature of the I2 deletion mutant and the VMAP mutants is a block in morphogenesis and failure to form membranes lacking the D13 scaffold. Pulse-chase experiments indicated that the L1 and F9 EFC proteins made by the I2L deletion mutant were less stable than proteins made by WT virus. We suggest that the EFC proteins normally insert into the viral membrane by a posttranslational mechanism after removal of the D13 scaffold and that the hydrophobicity of the EFC proteins contributes to their instability when this is prevented. The two major modes of protein degradation in eukaryotic cells are the ubiquitin-proteosome and autophagy-lysosomal pathways. We were unable to stabilize the EFC proteins with the proteasome inhibitor MG-132, which had to be administered at late times because of its other effects on VACV replication (data not shown). Whether either of the canonical pathways is involved in degradation of EFC proteins is currently uncertain.

In summary, the aberrant virus particles that form in the absence of I2 have numerous morphological defects, including a spherical shape, a poorly formed core, retention of the D13 scaffold, incomplete protein processing, and a deficiency in EFC proteins. The EFC deficiency likely prevents the entry of the aberrant particles into cells,

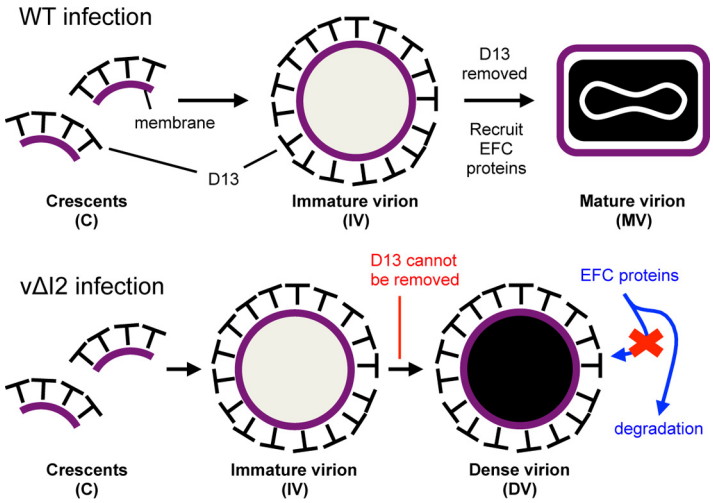

FIG 9 Model for defects caused by the absence of I2. During a WT VACV infection, crescent membranes coated with the D13 scaffold protein form and enlarge to form spherical immature virions containing the DNA and core proteins. Further morphogenesis involves processing of the A17 membrane protein by I7 proteinase, removal of the D13 scaffold, recruitment of the EFC proteins, and a change in shape. The immature virions also form during infection with the I2 deletion mutant vΔI2, but the D13 scaffold protein is not removed, and the change to the brick-shape with a well-defined core does not occur. Under these conditions, the EFC proteins fail to be inserted into the viral membrane and exhibit enhanced degradation.

but there is no evidence that I2 is an entry protein *per se*. A model to explain the defect in replication of the I2L deletion mutant is depicted in Fig. 9 and posits that the I2 protein is involved in the final stages of IV assembly or disassembly of the scaffold and that the deficiency of EFC proteins is secondary (Fig. 9). However, it is possible that I2 has multiple functions in association with the localization or activation of I7 proteinase or in chaperoning the EFC proteins.

MATERIALS AND METHODS

Cells and viruses. RK-13, RK-HA-I2, 293T, and BS-C-1 cells were grown in Dulbecco minimum essential medium or in minimum essential medium with Earle's balanced salts containing 10% fetal bovine serum (FBS; Sigma-Aldrich, St. Louis, MO), 2 mM L-glutamine, 100 U of penicillin, and 100 μg of streptomycin per ml (Quality Biologicals, Gaithersburg, MD). For RK-HA-I2 cells, 2 μg of puromycin/ml was included for antibiotic selection. The VACV Western Reserve strain (vWR) and recombinant VACV expressing the enhanced GFP fused to I2 (vGFP-I2) were propagated under standard conditions (25). The VACV I2L deletion mutant vΔI2 was propagated in RK-HA-I2 cells.

Construction of the RK-HA-I2 cell line. RK-HA-I2 cells were created using lentiviral transduction. A eukaryotic codon-optimized I2L ORF with an N-terminal HA tag (HA-I2) was cloned into pENTR-D-TOPO (Invitrogen, Carlsbad, CA) to generate pENTR-HA-I2. LR Clonase II (Invitrogen) was used to transfer HA-I2 from pENTR-HA-I2 into pLX302, yielding pLX302-HA-I2. Lentivirus particles were produced by cotransfecting pLX302-HA-I2 (transfer vector), psPAX2 (packaging vector), and pMD2.G (VSV-G envelope vector) into 293T cells using Lipofectamine 2000 (Invitrogen). psPAX2 (Addgene plasmid 12260) and pMD2.G (Addgene plasmid 12259) were from Didier Trono, and pLX302 (Addgene plasmid 25896) was from David Root (26). RK-13 cells were infected with the lentiviruses and passaged several times under selection with 2 μg of puromycin/ml. Puromycin-resistant cells were harvested and diluted to single cell per well in 96-well plates for clonal purification. Clones were tested for HA-I2 expression by Western blotting using anti-HA monoclonal antibody (MAb; data not shown), and the highest expressing RK-HA-I2 clone was chosen.

Formation of vΔI2 by homologous recombination. DNA encoding GFP regulated by the VACV P11 late promoter was inserted between left and right I2L ORF flanking sequences of approximately 500 bp using an In-Fusion HD cloning kit (Clontech, Mountain View, CA). RK-13 cells were infected with 1 PFU/cell of vWR, and transfected with the assembled DNA at 1 h postinfection (hpi) using Lipofectamine 2000 (Invitrogen). At 24 hpi, the cells were collected and lysed by rapid freeze-thaw cycles and sonication. Serial dilutions (10-fold) of the lysate were incubated with RK-HA-I2 cell monolayers, and plaques with green fluorescence were picked. Plaque purification was repeated five times to ensure clonal purity. A downstream forward primer (5′-CCGCGGCTAGTCCTATGTTGTATCAACTTC-3′) and upstream reverse primer (5′-ATGATATGTATGTCCATTAAAGTTAAATTGTGTAGCGCTTCT-3′) were used for PCR and sequencing to verify the deletion of the I2L ORF.

Construction of vGFP-I2. DNA containing the full-length I2L ORF with the N terminus fused to GFP (GFP-I2) was assembled with ~500 bp of I2L ORF flanking sequences into a plasmid using an In-Fusion HD cloning kit. The natural promoter of I2L was retained to regulate the expression of GFP-I2. RK-13 cells were infected with vWR and transfected with the assembled DNA for homologous recombination as described above. vGFP-I2 was clonally purified by repeated plaque picking in RK-13 cells and was sequenced to verify replacement of the I2L ORF with the GFP-I2 ORF.

Antibodies. The mouse MAb to human influenza virus HA tag (catalog no. MMS-101P) was obtained from Covance (Princeton, NJ). Mouse anti-glyceraldehyde-3-phosphate dehydrogenase MAb (Sc-32233) was from Santa Cruz Biotechnology, Dallas, TX, and rabbit anti-actin polyclonal antibody (PAb; A2066) was from Sigma-Aldrich. The rabbit PAbs used for VACV protein detection included rabbit antisera to A3 (unpublished data), A10 (unpublished data), A11 (10), A17-N (27), A21 (28), A27 (29), A28 (30), D13 (31), F9 (32), F10 (33), G3 (34), G7 (35), H2 (30), H3 (36), I7 (37), L1 (38), L5 (28), and vWR (18). Mouse MAbs to the A14 (39) and D8 (40) proteins were also used.

Purification of virus particles. vWR and vΔI2 virus particles were purified by sedimentation through a 36% sucrose cushion, followed by banding on a CsCl gradient. The gradient was formed by layering 1.3-g/ml (bottom, 3.5 ml), 1.25-g/ml (middle, 4 ml), and 1.2 g/ml (top, 3.5 ml) CsCl solutions containing 10 mM Tris-HCl and allowing diffusion overnight at 4°C. Sedimented virus material from the sucrose cushion was layered over the CsCl gradient and centrifuged for 4 h at 180,000 × *g* in a TH-641 rotor. The band of vΔI2 virus particles appeared to be slightly lower in the gradient than those of vWR, but the densities were not determined. The bands were recovered from the gradient, diluted 3-fold with 1 mM Tris-HCl (pH 9.0), and then pelleted by centrifugation.

Plaque assay and virus yield determination. BS-C-1, RK-13, and RK-HA-I2 cell monolayers were used for plaque assays in six-well plates. Virus samples were serially diluted in 10-fold increments and incubated with the monolayers at 37°C. After 1 h, the medium was aspirated and replaced with medium containing 0.5% methylcellulose. At 48 hpi, the cells were stained with crystal violet at room temperature for 10 min and dried overnight, and the plaques were counted.

Western blotting and signal quantification. Proteins from cells or purified virions were dissociated with NuPAGE (Life Technologies) lithium dodecyl sulfate buffer and reducing agent, resolved by electrophoresis on 4 to 12% NuPAGE Bis-Tris gels, and transferred to nitrocellulose membranes using an iBlot system (Life Technologies) as described previously (41). Membranes were blocked with 5% nonfat milk in Tris-buffered saline containing 0.05% Tween 20 or with Odyssey blocking buffer (Li-Cor Biosciences, Lincoln, NE) for 30 min to 1 h. Blocked membranes were incubated with the primary antibody for 1 h at room temperature or overnight at 4°C and then washed four times with the Tween buffer. Secondary antibody conjugated with IRDye 800CW or 680RD (Li-Cor Biosciences) was incubated with the membrane (1:10,000) for 1 h at room temperature, followed by four washes with the Tween buffer. The membranes were scanned using a Li-Cor Odyssey infrared imager, and the signal intensities of the bands were determined using Image Studio software (Li-Cor Biosciences).

Droplet digital PCR. RK-13 cells were infected with 10 PFU/cell of either vWR or vΔI2. At 10 hpi, mRNA was extracted from infected cells using TRIzol LS (Invitrogen), treated with DNase I (Invitrogen), and then reverse transcribed with SuperScript VILO MasterMix (Invitrogen). The cDNA was serially diluted and used as a template for droplet digital PCR (Bio-Rad, Hercules, CA). Following the manufacturer's protocol, the digital PCR was carried out with primers binding to individual ORFs. The following primer pairs were designed using PrimerQuest Tool from Integrated DNA Technologies, Coralville, IA (5′ to 3′): L1f (AACCATGGATGTAACCTCACTG) and L1r (TTCTGTAGCGGCTGATAACAC), L5f (AATACCCGATCCTATTG ATAGATTACG) and L5r (CGCAGATGTTTGAGTTGTCATC), A28f (ATGTAAAGCAAAAGTGGAGATGTG) and A28r (TGTTGCATCGTGTTAAATTTTCTAATG), G3f (ACTTCAGGCAGCTGTAATGGA) and G3r (CGACGGTTGAT GCATCGGTA), H2f (CAAGCTATTAGGCGAGGTACTG) and H2r (TGTTGAGCAGATGGATCGAC), A3f (GGCTAG ACCTATAAACGGCATC) and A3r (TTGATAGAAATCGGACTGTCGG), D8f (GTATAAATTGAACGACGACACGC) and D8r (TCTCAAATCGGACAACCATCTC), D13f (TCTATCCGGAGTTATGACAAACG) and D13r (GAATCTTCC CATACCTTTAACTTCTG), I2f (GCCGCTATATTTGGTGTATTTATGG) and I2r (AACCAATACCAACCCCAACA), I7f (AGGCGATAGACTTCTCACAAATG) and I7r (GCTCCTCTCTCAGGCTCTATT), and F10f (GTGGGCCATGGGATT AAACTA) and F10r (CAATGAGAGTTCCTGACCATCC). After 40 reaction cycles, the droplets were digitally analyzed with the droplet reader (Bio-Rad), and absolute mRNA copy numbers were determined.

Radioactive pulse-labeling and chase. RK-13 cells were infected with 5 PFU/cell of vWR or vΔI2 at 37°C. At 5.5 hpi, the cells were incubated with medium lacking methionine and cysteine and containing 2.5% dialyzed FBS for 30 min at 37°C. At 6 hpi, the cells were pulse-labeled at 37°C for 5 min with 100 μCi of [^{35}S]methionine-cysteine (Perkin-Elmer, Waltham, MA). Following the pulse, the cells were washed with phosphate-buffered saline (PBS), and the medium was changed to regular methionine-cysteine-containing medium for the chase. At various chase time points, the cells were washed with cold PBS and lysed with 1% NP-40 containing complete protease inhibitor cocktail (Roche Applied Science, Indianapolis, IN). The lysates were clarified by centrifugation and the proteins were captured with specific antibody and protein G Dynabeads (Life Technologies, Carlsbad, CA). The radiolabeled proteins were resolved in a 4 to 12% polyacrylamide gel, which was fixed in 40% methanol–10% acetic acid, soaked in 10% glycerol, dried, and exposed to a phosphor screen. A Typhoon variable mode imager (GE Healthcare, Chicago, IL) was used to detect radioactive bands.

Confocal microscopy. RK-13 cells were grown on coverslips in 24-well plates and infected with 3 PFU/cell of vGFP-I2. At 8 hpi, the cells were washed with PBS and fixed with 4% paraformaldehyde for 15 min at room temperature. The fixed cells were permeabilized with 0.1% Triton X-100 for 15 min and then blocked with 10% FBS for at least 30 min at room temperature. Primary antibodies were added at a 1:200 dilution in PBS containing 10% FBS for overnight at 4°C. The cells were washed and treated with

fluorescent dye-conjugated secondary antibodies (Alexa Fluor; Molecular Probes, Eugene, OR) at 1:200 dilution for at room temperature for 1 h. Subsequently, the cells were stained with 300 nM DAPI (Molecular Probes) (41). The coverslips were then mounted on a glass microscope slide with ProLong Gold antifade reagent (Molecular Probes). Confocal images were taken using Leica TCS SP5 microscope and processed with Imaris X64 7.6.1 software.

Transmission electron microscopy. Infected RK-13 or RK-HA-I2 cells in 60-mm plates were fixed with 2% glutaraldehyde in 0.1 M sodium cacodylate buffer, postfixed in 1% reduced osmium tetroxide, dehydrated in a series of ethanol incubations with final dehydrations in propylene oxide, and embedded in EmBed-812 resin (Electron Microscopy Sciences, Hatfield, PA) (42). The procedures for cryosectioning and immunogold labeling were described previously (43). Cryosections were picked up on grids, thawed, washed free of sucrose, stained with rabbit polyclonal D13 antibody, and then protein A conjugated to 10-nm gold spheres (University Medical Center, Utrecht, Netherlands). For purified virus particles, a 15-μl drop was placed on a Formvar-coated grid for 1 min and washed several times with 1 mM Tris-HCl (pH 9.0). A drop of 7% uranyl acetate in 50% ethanol was placed on grid for 30 s and then wicked off. Specimens were viewed with an FEI Tecnai Spirit transmission electron microscope (FEI, Hillsboro, OR).

ACKNOWLEDGMENTS

We thank Cindy Wolfe for the results of preliminary experiments and Catherine Cotter for maintaining cell lines. S. Shuman, Y. Xiang, and G. L. Smith kindly provided antibodies.

Funding was provided by the Division of Intramural Research, National Institute of Allergy and Infectious Disease, National Institutes of Health.

REFERENCES

1. Moss B. 2013. Poxviridae, p 2129–2159. *In* Knipe DM, Howley PM (ed), Fields virology, vol 2. Lippincott Williams & Wilkins, Philadelphia, PA.
2. Condit RC, Moussatche N, Traktman P. 2006. In a nutshell: structure and assembly of the vaccinia virion. Adv Virus Res 66:31–124. https://doi.org/10.1016/S0065-3527(06)66002-8.
3. Yoder JD, Chen TS, Gagnier CR, Vemulapalli S, Maier CS, Hruby DE. 2006. Pox proteomics: mass spectrometry analysis and identification of vaccinia virion proteins. Virol J 3:10. https://doi.org/10.1186/1743-422X-3-10.
4. Chung CS, Chen CH, Ho MY, Huang CY, Liao CL, Chang W. 2006. Vaccinia virus proteome: identification of proteins in vaccinia virus intracellular mature virion particles. J Virol 80:2127–2140. https://doi.org/10.1128/JVI.80.5.2127-2140.2006.
5. Resch W, Hixson KK, Moore RJ, Lipton MS, Moss B. 2007. Protein composition of the vaccinia virus mature virion. Virology 358:233–247. https://doi.org/10.1016/j.virol.2006.08.025.
6. Ngo T, Mirzakhanyan Y, Moussatche N, Gershon PD. 2016. Primary structures of the virion proteins of vaccinia virus at increased resolution. J Virol 90:9905–9919. https://doi.org/10.1128/JVI.01042-16.
7. Senkevich TG, Ojeda S, Townsley A, Nelson GE, Moss B. 2005. Poxvirus multiprotein entry-fusion complex. Proc Natl Acad Sci U S A 102:18572–18577. https://doi.org/10.1073/pnas.0509239102.
8. Moss B. 2016. Membrane fusion during poxvirus entry. Semin Cell Dev Biol 60:89–96. https://doi.org/10.1016/j.semcdb.2016.07.015.
9. Nichols RJ, Stanitsa E, Unger B, Traktman P. 2008. The vaccinia I2L gene encodes a membrane protein with an essential role in virion entry. J Virol 82:10247–10261. https://doi.org/10.1128/JVI.01035-08.
10. Resch W, Weisberg AS, Moss B. 2005. Vaccinia virus nonstructural protein encoded by the A11R gene is required for formation of the virion membrane. J Virol 79:6598–6609. https://doi.org/10.1128/JVI.79.11.6598-6609.2005.
11. Maruri-Avidal L, Weisberg AS, Moss B. 2013. Association of the vaccinia virus A11 protein with the endoplasmic reticulum and crescent precursors of immature virions. J Virol 87:10195–11206. https://doi.org/10.1128/JVI.01601-13.
12. Holzer G, Falkner FG. 1997. Construction of a vaccinia virus deficient in the essential DNA repair enzyme uracil DNA glycosylase by a complementing cell line. J Virol 71:4997–5002.
13. Warren RD, Cotter C, Moss B. 2012. Reverse genetic analysis of poxvirus intermediate transcription factors. J Virol 86:9514–9519. https://doi.org/10.1128/JVI.06902-11.
14. Heuser J. 2005. Deep-etch EM reveals that the early poxvirus envelope is a single membrane bilayer stabilized by a geodetic "honeycomb" surface coat. J Cell Biol 169:269–283. https://doi.org/10.1083/jcb.200412169.
15. Szajner P, Weisberg AS, Lebowitz J, Heuser J, Moss B. 2005. External scaffold of spherical immature poxvirus particles is made of protein trimers, forming a honeycomb lattice. J Cell Biol 170:971–981. https://doi.org/10.1083/jcb.200504026.
16. Bisht H, Weisberg AS, Szajner P, Moss B. 2009. Assembly and disassembly of the capsid-like external scaffold of immature virions during vaccinia virus morphogenesis. J Virol 83:9140–9150. https://doi.org/10.1128/JVI.00875-09.
17. Unger B, Mercer J, Boyle KA, Traktman P. 2013. Biogenesis of the vaccinia virus membrane: genetic and ultrastructural analysis of the contributions of the A14 and A17 proteins. J Virol 87:1083–1097. https://doi.org/10.1128/JVI.02529-12.
18. Davies DH, Wyatt LS, Newman FK, Earl PL, Chun S, Hernandez JE, Molina DM, Hirst S, Moss B, Frey SE, Felgner PL. 2008. Antibody profiling by proteome microarray reveals the immunogenicity of the attenuated smallpox vaccine modified vaccinia virus Ankara is comparable to that of Dryvax. J Virol 82:652–663. https://doi.org/10.1128/JVI.01706-07.
19. Maruri-Avidal L, Weisberg AS, Bisht H, Moss B. 2013. Analysis of viral membranes formed in cells infected by a vaccinia virus L2-deletion mutant suggests their origin from the endoplasmic reticulum. J Virol 87:1861–1871. https://doi.org/10.1128/JVI.02779-12.
20. Maruri-Avidal L, Weisberg AS, Moss B. 2013. Direct formation of vaccinia virus membranes from the endoplasmic reticulum in the absence of the newly characterized L2-interacting protein A30.5. J Virol 87:12313–12326. https://doi.org/10.1128/JVI.02137-13.
21. Wolffe EJ, Vijaya S, Moss B. 1995. A myristylated membrane protein encoded by the vaccinia virus L1R open reading frame is the target of potent neutralizing monoclonal antibodies. Virology 211:53–63. https://doi.org/10.1006/viro.1995.1378.
22. Satheshkumar PS, Weisberg A, Moss B. 2009. Vaccinia virus H7 protein contributes to the formation of crescent membrane precursors of immature virions. J Virol 83:8439–8450. https://doi.org/10.1128/JVI.00877-09.
23. Meng X, Embry A, Rose L, Yan B, Xu C, Xiang Y. 2012. Vaccinia virus A6 is essential for virion membrane biogenesis and localization of virion membrane proteins to sites of virion assembly. J Virol 86:5603–5613. https://doi.org/10.1128/JVI.00330-12.
24. Meng X, Wu X, Yan B, Deng J, Xiang Y. 2013. Analysis of the role of vaccinia virus H7 in virion membrane biogenesis with an H7 deletion mutant. J Virol 87:8247–8253. https://doi.org/10.1128/JVI.00845-13.
25. Cotter CA, Earl PL, Wyatt LS, Moss B. 2017. Preparation of cell cultures and vaccinia virus stocks. Curr Protoc Mol Biol 117:16.16.1–16.16.18. https://doi.org/10.1002/cpmb.33.
26. Yang X, Boehm JS, Salehi-Ashtiani K, Hao T, Shen Y, Lubonja R, Thomas SR, Alkan O, Bhimdi T, Green TM, Johannessen CM, Silver SJ, Nguyen C, Murray RR, Hieronymus H, Balcha D, Fan C, Lin C, Ghamsari L, Vidal M, Hahn WC, Hill DE, Root DE. 2011. A public genome-scale lentiviral

expression library of human ORFs. Nat Methods 8:659–661. https://doi.org/10.1038/nmeth.1638.
27. Betakova T, Wolffe EJ, Moss B. 1999. Regulation of vaccinia virus morphogenesis: phosphorylation of the A14L and A17L membrane proteins and C-terminal truncation of the A17L protein are dependent on the F10L protein kinase. J Virol 73:3534–3543.
28. Townsley A, Senkevich TG, Moss B. 2005. Vaccinia virus A21 virion membrane protein is required for cell entry and fusion. J Virol 79:9458–9469. https://doi.org/10.1128/JVI.79.15.9458-9469.2005.
29. Howard AR, Senkevich TG, Moss B. 2008. Vaccinia virus A26 and A27 proteins form a stable complex tethered to mature virions by association with the A17 transmembrane protein. J Virol 82:12384–12391. https://doi.org/10.1128/JVI.01524-08.
30. Nelson GE, Sisler JR, Chandran D, Moss B. 2008. Vaccinia virus entry/fusion complex subunit A28 is a target of neutralizing and protective antibodies. Virology 380:394–401. https://doi.org/10.1016/j.virol.2008.08.009.
31. Sodeik B, Griffiths G, Ericsson M, Moss B, Doms RW. 1994. Assembly of vaccinia virus: effects of rifampin on the intracellular distribution of viral protein p65. J Virol 68:1103–1114.
32. Brown E, Senkevich TG, Moss B. 2006. Vaccinia virus F9 virion membrane protein is required for entry but not virus assembly, in contrast to the related L1 protein. J Virol 80:9455–9464. https://doi.org/10.1128/JVI.01149-06.
33. Szajner P, Weisberg AS, Moss B. 2004. Evidence for an essential catalytic role of the F10 protein kinase in vaccinia virus morphogenesis. J Virol 78:257–265. https://doi.org/10.1128/JVI.78.1.257-265.2004.
34. Wagenaar TR, Ojeda S, Moss B. 2008. Vaccinia virus A56/K2 fusion regulatory protein interacts with the A16 and G9 subunits of the entry fusion complex. J Virol 82:5153–5160. https://doi.org/10.1128/JVI.00162-08.
35. Szajner P, Jaffe H, Weisberg AS, Moss B. 2003. Vaccinia virus G7L protein interacts with the A30L protein and is required for association of viral membranes with dense viroplasm to form immature virions. J Virol 77:3418–3429. https://doi.org/10.1128/JVI.77.6.3418-3429.2003.
36. Da Fonseca FG, Weisberg A, Wolffe EJ, Moss B. 2000. Characterization of the vaccinia virus H3L envelope protein: topology and posttranslational membrane insertion via the C-terminal hydrophobic tail. J Virol 74:7508–7517. https://doi.org/10.1128/JVI.74.16.7508-7517.2000.
37. Kane EM, Shuman S. 1993. Vaccinia virus morphogenesis is blocked by a temperature-sensitive mutation in the I7 gene that encodes a virion component. J Virol 67:2689–2698.
38. Lustig S, Fogg C, Whitbeck JC, Eisenberg RJ, Cohen GH, Moss B. 2005. Combinations of polyclonal or monoclonal antibodies to proteins of the outer membranes of the two infectious forms of vaccinia virus protect mice against a lethal respiratory challenge. J Virol 79:13454–13462. https://doi.org/10.1128/JVI.79.21.13454-13462.2005.
39. Meng X, Zhong Y, Embry A, Yan B, Lu S, Zhong G, Xiang Y. 2011. Generation and characterization of a large panel of murine monoclonal antibodies against vaccinia virus. Virology 409:271–279. https://doi.org/10.1016/j.virol.2010.10.019.
40. Parkinson JE, Smith GL. 1994. Vaccinia virus gene A36R encodes a M_r 43-50 K protein on the surface of extracellular enveloped virus. Virology 204:376–390. https://doi.org/10.1006/viro.1994.1542.
41. Hyun SI, Maruri-Avidal L, Moss B. 2015. Topology of endoplasmic reticulum-associated cellular and viral proteins determined with split-GFP. Traffic 16:787–795. https://doi.org/10.1111/tra.12281.
42. Maruri-Avidal L, Domi A, Weisberg AS, Moss B. 2011. Participation of vaccinia virus L2 protein in the formation of crescent membranes and immature virions. J Virol 85:2504–2511. https://doi.org/10.1128/JVI.02505-10.
43. Senkevich TG, Wyatt LS, Weisberg AS, Koonin EV, Moss B. 2008. A conserved poxvirus NlpC/P60 superfamily protein contributes to vaccinia virus virulence in mice but not to replication in cell culture. Virology 374:506–514. https://doi.org/10.1016/j.virol.2008.01.009.